BJRS
BRAZILIAN JOURNAL OF RADIATION SCIENCES

org/10.15392/2319-0612.2026.3058
Braz. J. Radiat. Sci., Rio de Janeiro
Oct-Dec 2026, 14(4) | 01-19 | e3058
Editor(s): Dr. (Prof.) Bernardo Maranhão Dantas
Dr. (Prof.) Alfredo L. Ferreira Filho
Submitted: 2026-06-01-30
Accepted: 2026-06-03

Original Article

Influence of the volume of laboratory-developed simulators on the counting efficiency (kCPS/MBq) of the PET scanner belonging to LIM/CDTN

Silva[a,b*], A. V.; Gontijo [a,b,c], R. M. G.; Mendes[a], B.M.; Ferreira[a], A. V.

[a] CNEN/CDTN - Centro de Desenvolvimento da Tecnologia Nuclear, 31270-901, Belo Horizonte, Minas Gerais, Brasil..

[b] FM/Federal University of Minas Gerais, 30130-100, Belo Horizonte, Minas Gerais, Brasil.
[c] EBSERH - Empresa Brasileira de Serviços Hospitalares, 30130-190, Belo Horizonte, Minas Gerais, Brasil.

*Correspondence: Ilexysilva@gmail.com

Abstract: This study investigated the influence of phantom volume on the conversion coefficient between count rate (CPS) and activity (MBq) for a preclinical Positron Emission Tomography (PET) scanner, the Triumph® LabPET Solo 4, installed at the LIM/CDTN (*Laboratório de Imagem Molecular do Centro de Desenvolvimento da Tecnologia Nuclear*). Three cylindrical phantoms (S, M, and L) with different internal volumes (17.7 mL, 22.0 mL, and 26.5 mL, respectively) were fabricated. PET images were acquired using two approaches: spatial and temporal. The spatial acquisition mode was used to verify the quality and homogeneity of the reconstructed PET images for the different phantom volumes. In this analysis, no relevant variations in image quality were observed among the phantoms. The temporal acquisition mode was applied to evaluate the behavior of count rates as a function of activity, analyzing total, true, random, scattered, and noise-equivalent count (NEC). The results demonstrated a progressive reduction in counting efficiency with increasing phantom volume, indicating an inverse relationship between phantom size and detection efficiency. These findings emphasize the importance of considering phantom geometry in calibration and quantitative procedures in preclinical PET imaging studies to ensure accurate measurements.

Keywords: PET imaging, conversion factor, mouse phantom, count rate.

SBPR

Copyright © 2026 Authors.

OPEN ACCESS

CC BY

BJRS
BRAZILIAN JOURNAL OF RADIATION SCIENCES

doi.org/10.15392/2319-0612.2026.3058
Braz. J. Radiat. Sci., Rio de Janeiro
Oct-Dec 2026, 14(4) | 01-19 | e3058
Editor(s): Dr. (Prof.) Bernardo Maranhão Dantas
Dr. (Prof.) Alfredo L. Ferreira Filho
Submitted: 2026-06-01-30
Accepted: 2026-06-03

Influência do volume de simuladores desenvolvidos em laboratório na eficiência de contagem (kCPS/MBq) do Tomógrafo PET pertencente ao LIM/CDTN

Resumo: Este estudo investigou a influência do volume do simulador no coeficiente de conversão entre a taxa de contagem (kCPS) e a atividade (MBq) para um tomógrafo de Tomografia por Emissão de Pósitrons (PET) pré-clínico, o Triumph® LabPET Solo 4, instalado no LIM/CDTN (Laboratório de Imagem Molecular do Centro de Desenvolvimento da Tecnologia Nuclear). Três simuladores cilíndricos (S, M e L), com diferentes volumes internos (17.7 mL, 22.0 mL, e 26.5 mL, respectivamente), foram confeccionados. As imagens PET foram adquiridas utilizando duas abordagens: espacial e temporal. O modo de aquisição espacial foi utilizado para verificar a qualidade e a homogeneidade das imagens PET reconstruídas para os diferentes volumes dos simuladores. Nessa análise, não foram observadas variações relevantes na qualidade da imagem entre os simuladores. O modo de aquisição temporal foi aplicado para avaliar o comportamento das taxas de contagem em função da atividade, analisando as contagens totais, verdadeiras, aleatórias, espalhadas e as contagens equivalentes de ruído (NEC). Os resultados demonstraram uma redução progressiva da eficiência de contagem com o aumento do volume do simulador, indicando uma relação inversa entre o tamanho do simulador e a eficiência de detecção. Esses achados reforçam a importância de considerar a geometria do simulador nos procedimentos de calibração e quantificação em estudos de imagem PET pré-clínica, a fim de garantir medições mais precisas.

Palavras-chave: imagem PET, fator de conversão, simulador de camundongo, taxa de contagem.

SBPR

Copyright © 2026 Authors.

OPEN ACCESS

CC BY

1. INTRODUCTION

Positron Emission Tomography (PET) detects two 511 keV photons emitted simultaneously after the annihilation of a positron. These photons, originating from the administered radiopharmaceutical, are captured within a time window (12 nanoseconds) and must be aligned in a straight line between two detectors, called the LOR (Line of Response) [1].

The coincidence events detected by the scanner include true, random, and scattered events, as illustrated in Figure 1.

Figure 1: Types of coincidence events detected by the scanner:
A) True; B) Scattered; C) Random.

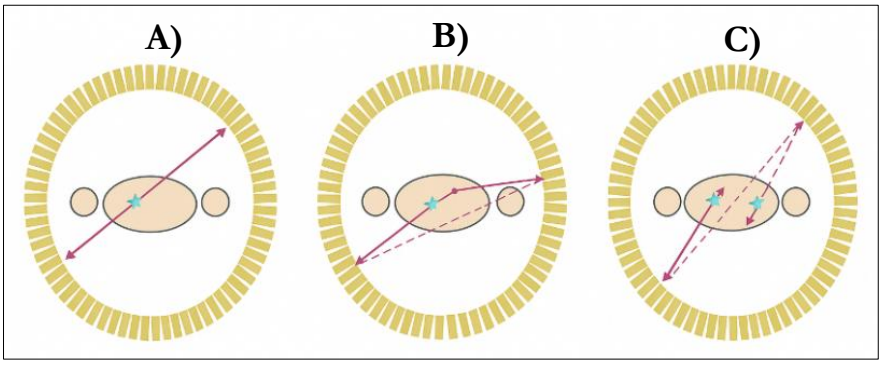

Source: Adapted from Saha, 2010.

True events occur when two photons from the same annihilation are detected within the coincidence window. This allows a LOR to be traced between the detectors, directly contributing to the real location of the annihilation event and therefore affects image quality [1].

Scattered events occur when one or both photons undergo deflection by the Compton effect after annihilation, generating incorrect LORs, could increase background noise, and reduce image quality [1].

Random events occur when photons from different annihilations are detected as if they were from the same event. This generates false LORs that do not correspond to the actual distribution of the radiopharmaceutical, impairing image quality [1].

OPEN ACCESS

A study conducted in 2019 [2] determined the distribution of coincidence events for the small-animal PET scanner at the *Laboratório de Imagem Molecular do Centro de Desenvolvimento da Tecnologia Nuclear (LIM/CDTN)*, using a mouse phantom (height 5.75 mm; diameter 2.88 mm) filled with Rad'ioglic® (^{18}F-FDG radiopharmaceutical). Figure 2 shows the results of this study and the phantom used.

Figure 2: A) Image of the graph showing the distribution of coincidence events from the small-animal PET scanner at LIM/CDTN.; B) Mouse Phantom

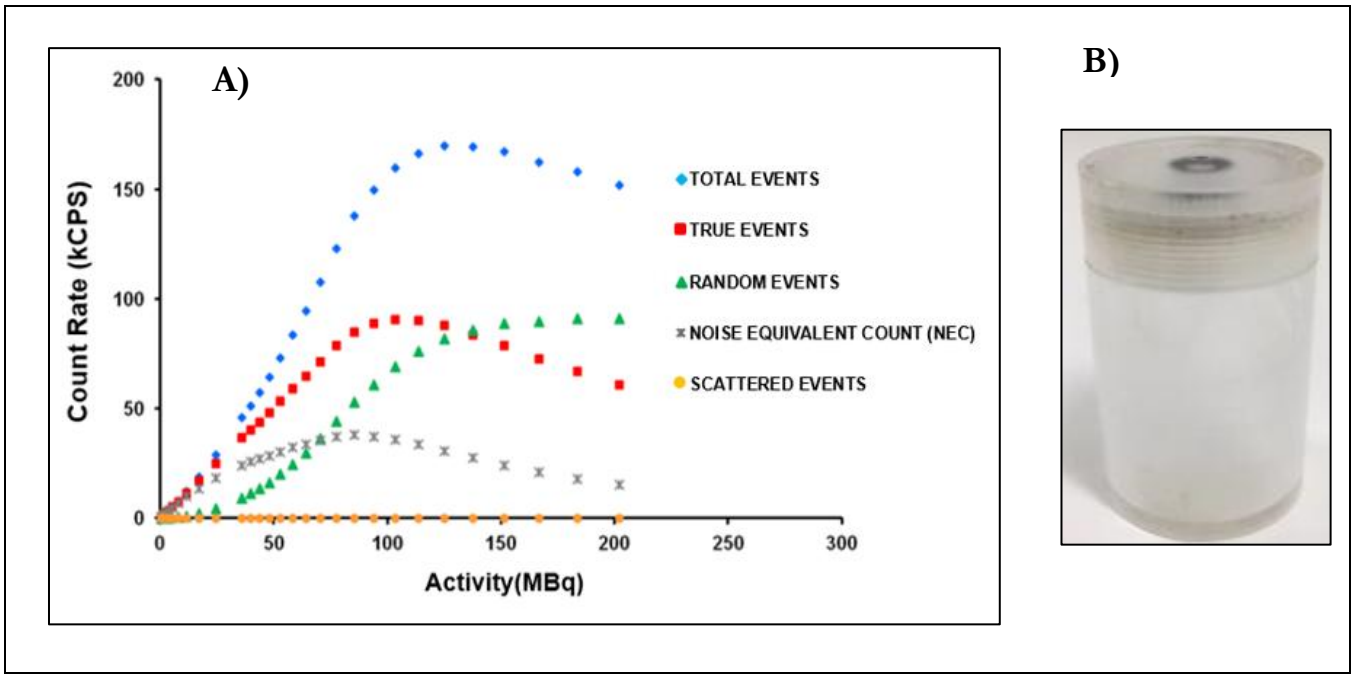

Source: Extracted from Gontijo, *et al* (2019).

The mouse phantom, Figure 2B, is routinely used at LIM for determining the conversion coefficient from count rate (CPS) to activity (MBq).

It is important to note that the distribution of PET coincidence events depends on the geometry of the imaged object. Therefore, it is expected that phantoms with different geometries will lead to different CPS/MBq conversion coefficients.

According to MacDonald *et al.* (2011),

> The noise equivalent count (NEC) parameter is a measure of valid ("true") coincident events relative to unwanted scattered and accidental coincidence events recorded by the scanner and has been widely used as a measure of effective count sensitivity in PET scanners [3].

OPEN ACCESS

Accordingly, this study aims to investigate the influence of mouse simulator geometry on the counting efficiency (CPS/MBq) of a PET scanner dedicated to small animals at LIM/CDTN.

2. MATERIALS AND METHODS

2.1. MATERIALS

The materials used for the development of this work were: (i) Transparent cylindrical acrylic tube and rod; (ii) Mechanical lathe for machining; (iii) Chloroform and sandpaper for finishing; (iv) Cylindrical phantoms; (v) Precision analytical balance (BEL Mark 210A, readability of 0.001 g); (vi) ^{18}F-FDG radiopharmaceutical (Fluorodeoxyglucose); (vii) Capintec CRC-25 activimeter; (viii) Triumph® LabPET Solo 4 dedicated small-animal PET scanner; (ix) Amide® and Microsoft Excel® (Microsoft 365) software for image and data analysis. The main materials used are shown in Figures 3, 4, and 5.

OPEN ACCESS

Figure 3: A) Machining lathe; B) 18F-FDG radiopharmaceutical – Radioglic®; C) Capintec CRC-25 activimeter; D) Precision analytical balance (BEL Engineering®, Mark 210A)

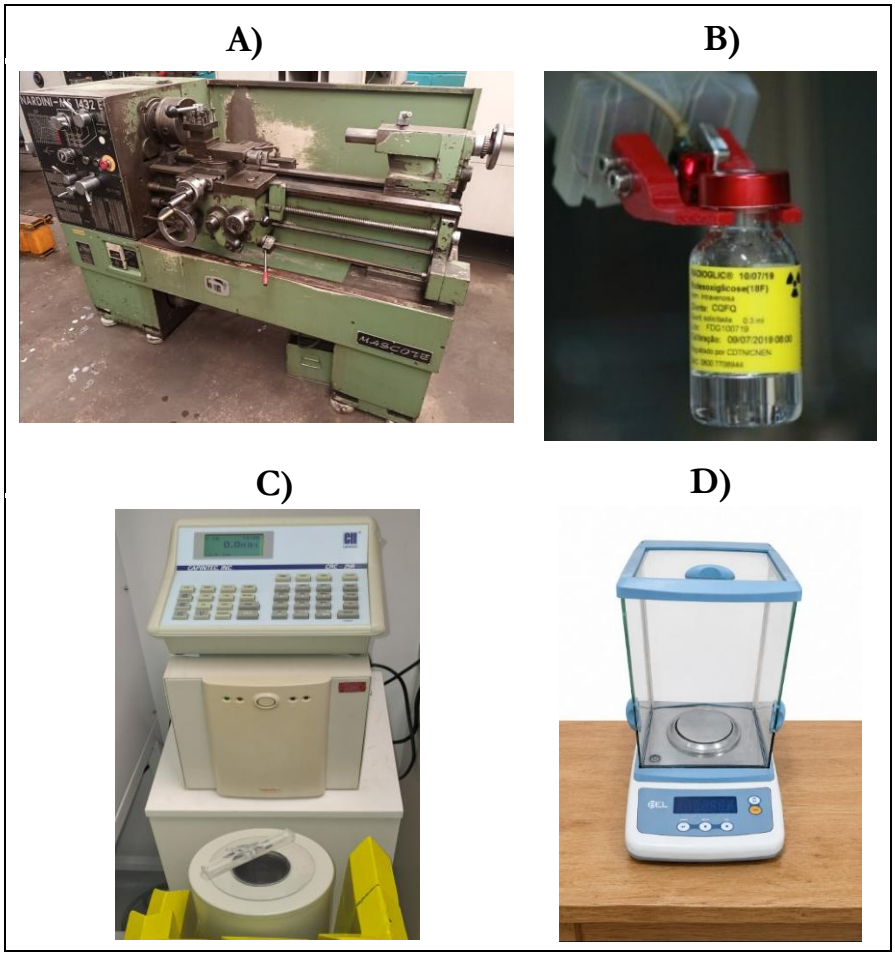

Source: authors.

Figure 4: A) Transparent acrylic tube; B) Simulator covers; C) Transparent acrylic rod.

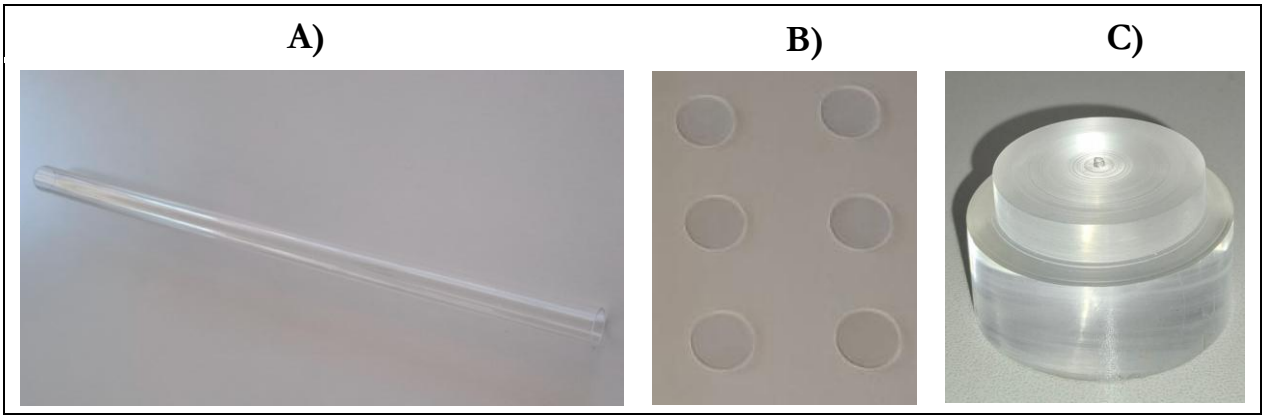

Source: authors.

OPEN ACCESS

Figure 5: MicroPET Scanner Triumph® LabPET Solo 4



Source: authors.

2.2. Methods

2.2.1. Phantom Fabrication

The first stage of the work consisted of fabricating cylindrical phantoms from a commercial acrylic tube. Three phantoms S, M and L (Small, Medium, and Large, respectivelly) were fabricated, with internal volumes differing by approximately 20% between them, from the smallest to the largest.

Phantoms were fabricated with the technical assistance of Dr. Eduardo Sarmento Valente, from the *Serviço de Radiofármacos* (SERFA/CDTN), whose expertise in operating the mechanical lathe was essential for the reproducibility and precision of the pieces. The caps for the phantoms were made from an acrylic rod and machined to the appropriate shape, as shown in Figure 4A and 4B.

After machining the pieces, the caps were attached to the bodies of the phantoms and bonded using chloroform, a chemical agent that reacts with acrylic, allowing the pieces to be sealed.

OPEN ACCESS

To ensure the integrity of the phantoms and prevent leakage of radioactive material during the experiments, a sealing test was performed after bonding. The test involved filling the phantoms with water and then placing them on absorbent paper, allowing the detection of any leaks, which would indicate sealing failures. At the end of the test, no irregularities were observed, confirming the suitability of the phantoms for the subsequent experiments.

2.2.2. Determination of the volumes of the phantoms

In order to verify the equivalence between the actual internal volumes of the fabricated phantoms and the theoretical volumes previously estimated through geometric calculations, tests were conducted using a precision analytical balance. Each of the three cylindrical phantoms was weighed individually under two conditions: (i) empty and (ii) completely filled with distilled water. For each condition, five consecutive measurements were performed to ensure data repeatability and minimize potential experimental variations.

The internal volume was determined from the mass difference between the filled and empty phantom, considering the density of water as 1 g/mL at room temperature (approximately 25 °C), which allowed the direct conversion of the water mass into volume.

2.2.3. PET Image Acquisition

The phantoms were filled with a solution of 18F-FDG diluted in Milli-Q water. Homogenization of the radioactive solution was performed using a vortex mixer prior to image acquisition, ensuring a uniform distribution of activity within the phantom.

PET images were acquired using two distinct acquisition modes: (i) temporal, in which the phantom remains in a single position throughout the entire acquisition period, and (ii) spatial, in which the phantom is positioned at multiple locations across the field of view (FOV). In the spatial mode, the object's movement is simulated through discrete repositioning of the phantom between acquisitions, representing stepwise displacements (1.8 cm) along the axial direction, analogous to table motion in clinical multi-bed PET imaging.

OPEN ACCESS

Each position corresponds to a distinct "bed position," with a fixed acquisition time per bed. No continuous motion is applied during the acquisition. The experimental parameters used for image acquisition are summarized in Tables 1 and 2.

Table 1: Parameters of temporal and spatial acquisition modes

ACTION	PARAMETER	MODE	
		TEMPORAL	SPATIAL
3D Aquisition	Time	8 hours	15 minutes*
	Bed positions	1	5
	Resolution	Standart	
	Initial activity** (MBq)	190	S: 40.9
			M: 45.2
			L: 48.1
	FOV diameter	60 mm	
	FOV axial lenght	3.7 mm	

*Total scan duration; **Acquisition Beginning.

Table 2: Reconstruction parameters of temporal and spatial images

ACTION	PARAMETER	MODE	
		TEMPORAL	SPATIAL
Reconstruction	Algorithm	MLEM-3D	
	Number of iterations	20	
	Analyzed frames	19	--
	Frame duration	10 seconds	--
	Activity diference between frames	10 MBq	--

2.2.4. Image Analysis

The images were reconstructed using the parameters described in Table 2 according to the corresponding acquisition mode (temporal or spatial).

In the spatial acquisition mode, the reconstructed images were qualitative analysed to ensure the quality formation of the PET image obtained by the scanner.

OPEN ACCESS

In the images acquired in the temporal mode, the procedure for evaluating the scanner count rates, as described in the NEMA NU 4/2008 publication [4], could not be fully applied, since the LabPET 1.12 software provided by the manufacturer does not allow access to the sinograms. However, information on the counted events is available in text files (.txt) for: (i) true events, (ii) random events, (iii) scattered events, and (iv) total events.

For each analyzed frame of the images acquired in the temporal mode, the counts recorded by the software were analyzed to evaluate the count rate performance of the PET scanner using the cylindrical phantom. It is important to note that the LabPET SOLO 4 model used in this study does not perform attenuation or scatter corrections.

The noise-equivalent count (NEC) values were calculated according to Equation (1).

$$\mathbf{NEC} = \frac{\mathbf{T^2}}{\mathbf{T+R+S}} \qquad (1)$$

Where T represents true events, R represents random events, and S represents scattered events [5]. Data was organized in Microsoft Excel® spreadsheets, enabling the analysis of total, true, random, and scattered counts for each time interval.

3. RESULTS AND DISCUSSIONS

3.1. Phantom Fabrication and Internal Volume Verification

Three phantoms (S, M, and L), with variations in height and constant diameter, were successfully fabricated and are shown in Figure 6.

OPEN ACCESS

Figure 6: Side-by-side comparison of the three phantoms

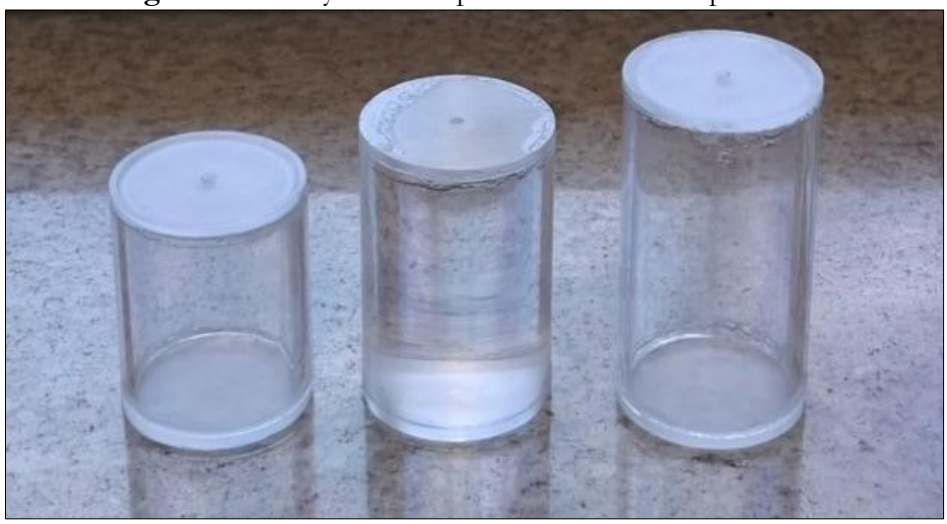

Source: authors.

The mean masses obtained for the phantoms completely filled with water were 27.6529 g (S), 33.8361 g (M) and 40.0461 g (L), while the corresponding masses of the empty phantoms were 10.0027 g (S), 11.8588 g (M) and 13.5761 g (L). The difference between the filled and empty masses resulted in 17.6502 g (S), 21.9773 g (M) and 26.4700 g (L), with standard deviations below 0.0002 g, indicating high repeatability of the measurements.

Table 3 shows the overall dimensions of the three phantoms, with the volume calculated assuming the density of water is 1 g/cm³.

Table 3: Characteristics of the Cylindrical Phantoms

PHANTOMS			
SIZE	**HEIGHT (mm)**	**DIAMETER (mm)**	**VOLUME* (mL)**
S	33.00 ± 0.05	26.00 ± 0.05	17.7000 ± 0.0002
M	41.50 ± 0.05	26.00 ± 0.05	22.0000 ± 0.0002
L	49.80 ± 0.05	26.00 ± 0.05	26.5000 ± 0.0002

*Internal volume

OPEN ACCESS

3.2. Image Analysis – Spatial Mode

Figure 7 shows the PET images constructed from the spatial acquisition mode, highlighting the good image quality obtained by the scanner. This includes adequate geometric definition and homogeneous distribution of activity.

Figure 7: PET images reconstructed in spatial mode in the axial* and coronal** planes.
A) Phantom S; B) Phantom M; C) Phantom L

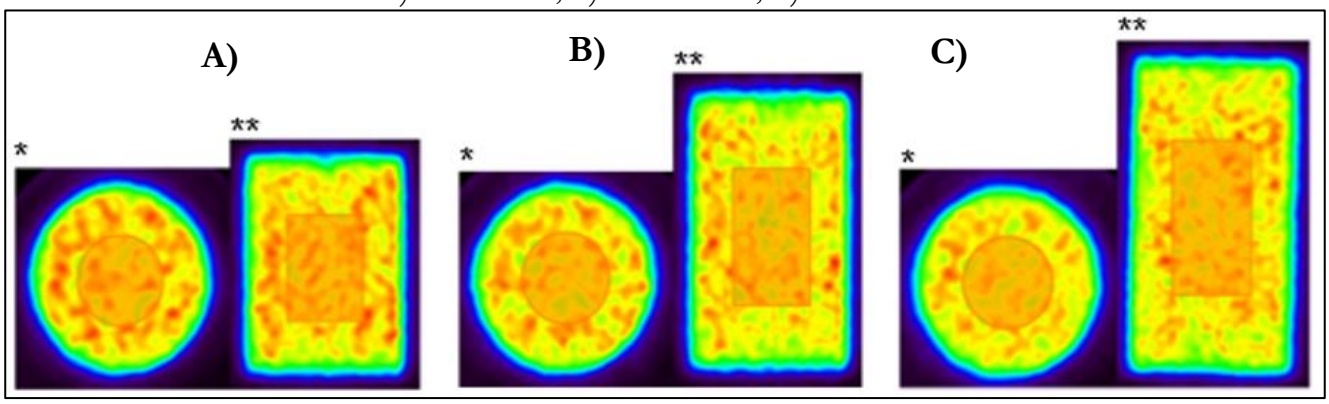

Source: authors.

3.3. Image Analysis – Temporal Mode

Following the acquisition of the images in the temporal mode, the .txt files were extracted and the data exported to Excel® to graphically evaluate the results. A reproducibility test was performed as a preliminary analysis, in which the scan of the M phantom was repeated to allow comparison of the results, to assess the reproducibility of the results, as shown in Figure 8 below. In this process, data normalization was also performed using the maximum value of the true events.

OPEN ACCESS

Figure 8: A) Analysis of count reproducibility in the temporal mode using the M phantom. B) Comparison based on the maximum value of the true events

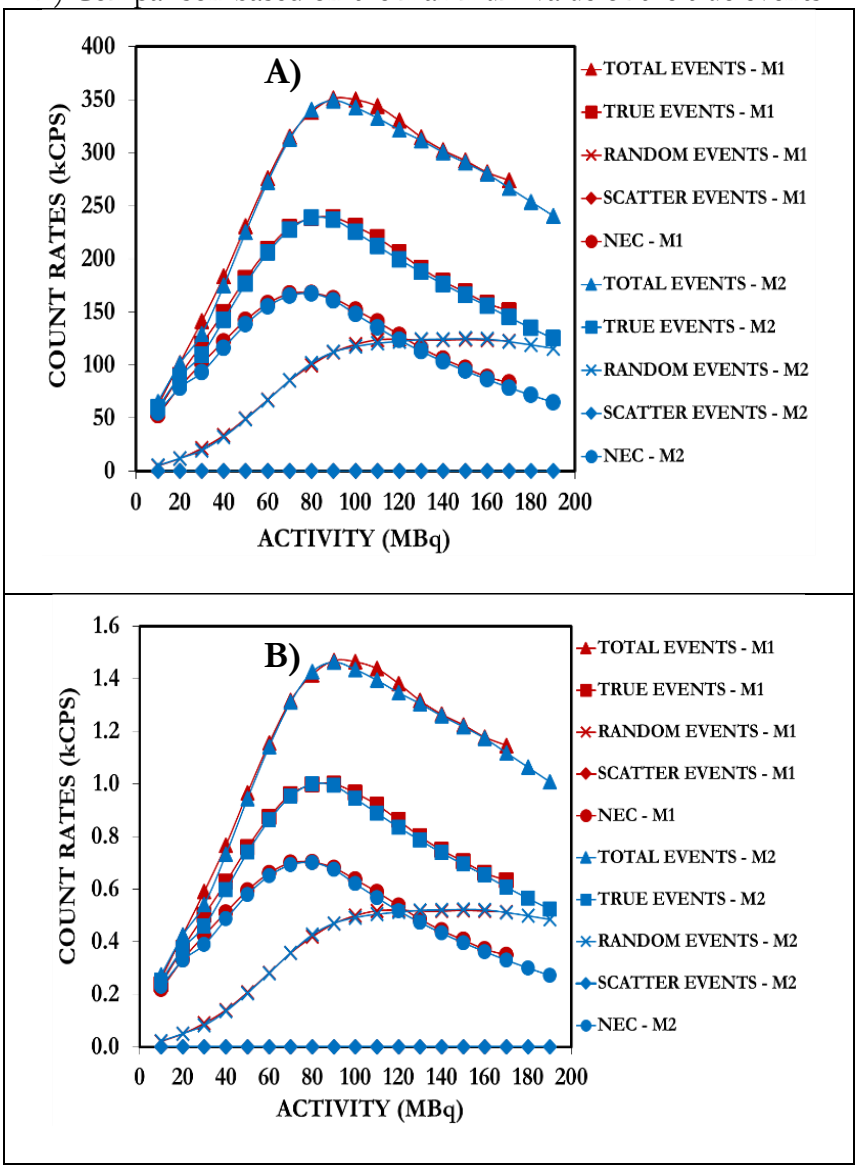

Source: authors.

The similar behavior between the curves demonstrates the reproducibility of the M phantom for the different acquisitions. Figure 9 shows representative graphs of the coincidence events generated for the three phantoms, S, M, and L.

OPEN ACCESS

Figure 9: A) Distribution of coincidence events;
B) Coincidence events normalized by the maximum value of the true events

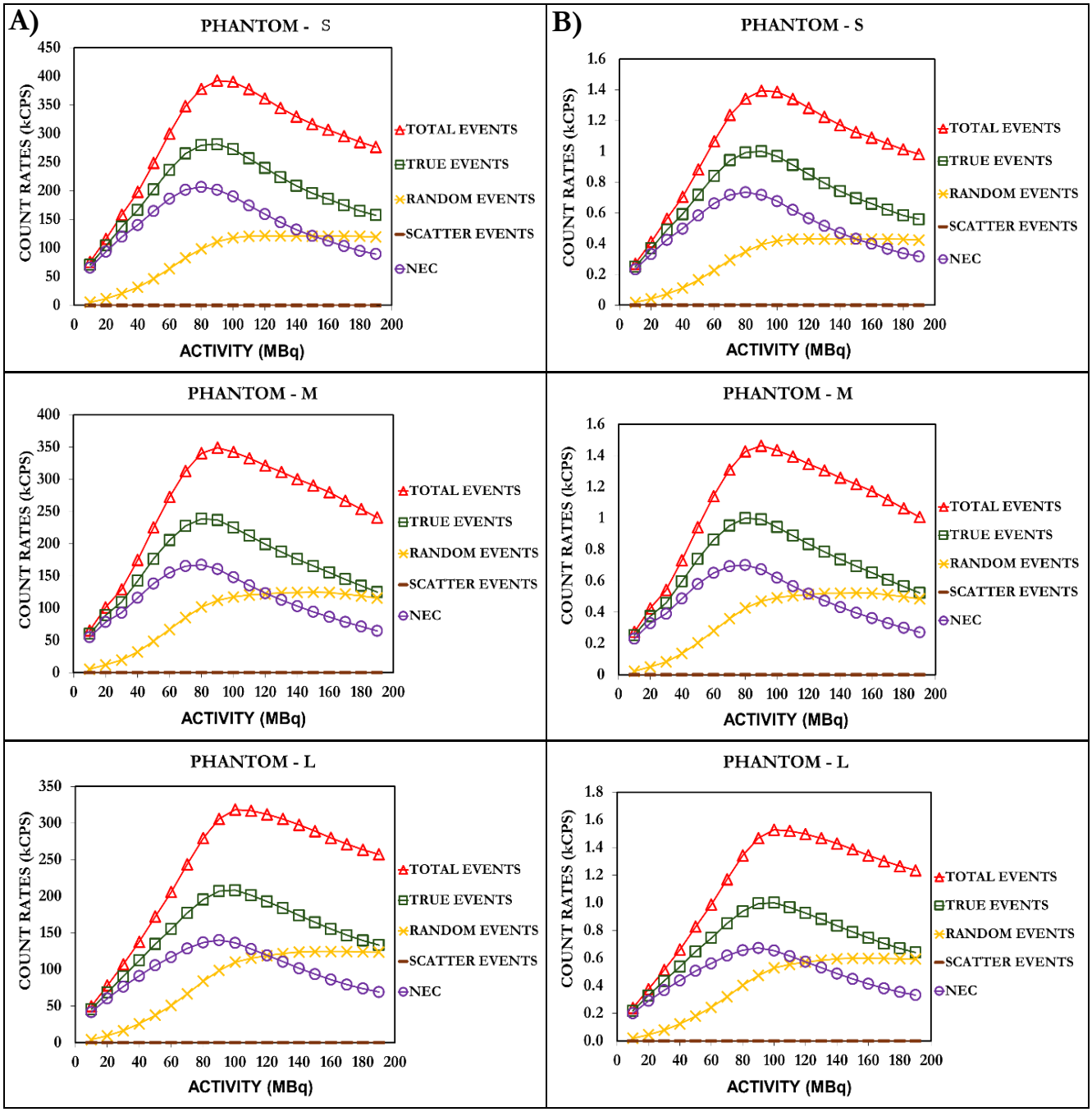

Source: authors.

For the graphical analysis of coincidence events, the total counts recorded for each type of event were initially considered. Subsequently, the data were normalized by dividing each value by the highest value observed among the true events. This approach allowed the data to be represented proportionally, facilitating comparison across the different event types.

OPEN ACCESS

The distribution of coincidence events showed appropriate and consistent behavior as expected. The values for true events are higher than those for other types of events throughout the acquisitions, indicating good system performance and quality of PET image acquisition.

To assess the saturation point of linearity in the three phantoms, graphs were generated from the data obtained in the images acquired. The graphical analysis reveals a progressive loss of count efficiency as the phantom size increases.

Thus, phantoms with larger volumes exhibit greater efficiency loss, demonstrating an inverse relationship between phantom size and detection efficiency in the temporal mode, as shown in Figure 10.

Figure 10: Linearity Curve Between True Events and Activity in the Temporal Mode

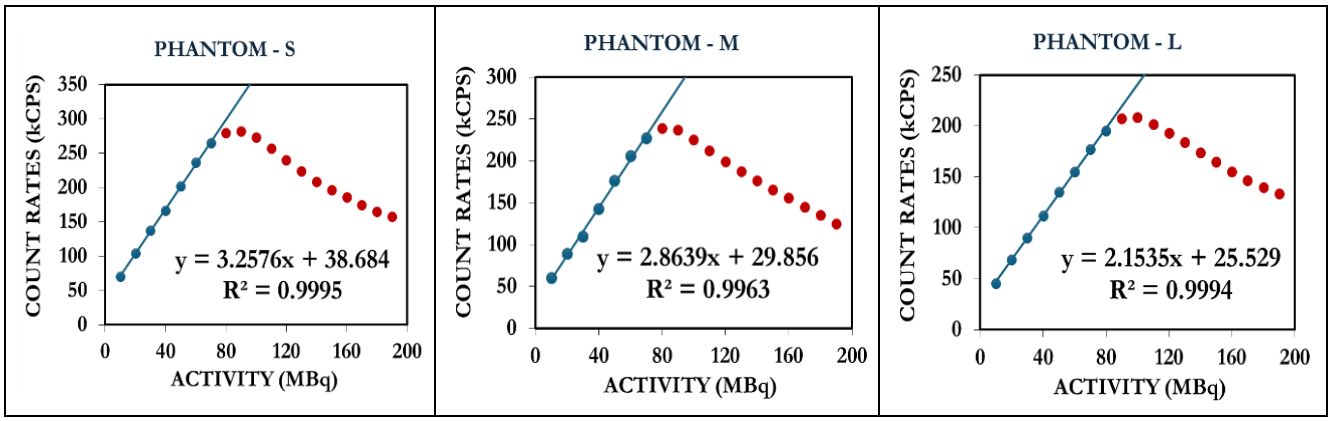

Source: authors.

The count efficiency values obtained for the S, M, and L phantoms were 3.26, 2.86, and 2.15 kCPS/MBq, respectively, as determined from the linear fits shown in Figure 10.

Based on these values, the relative differences in count efficiency between phantom sizes were calculated. A reduction of approximately 12.3% was observed from S to M, 24.8% from M to L, and 34.0% from S to L. These differences reflect the influence of phantom size (and consequently geometry) on the detected count rate, due to increased attenuation and scattering effects as the volume increases.

OPEN ACCESS

According to Gontijo, *et al* (2022) [6], the axial profile of absolute sensitivity of the PET used in this work revealed higher scanner sensitivity around the center of the FOV and decreasing sensitivity towards the ends of the FOV, as expected.

The conversion coefficient (kCPS/MBq) was determined from phantom acquisiton filled with known activity concentration using the same acquisition parameters as the phantoms in this study (S, M and L size).

The behavior observed in the curves presented in Figures 8, 9, and 10 can be explained based on the physical and electronic limitations of the detection system. The observed behaviors are related to dead-time and pulse pile-up effects, as well as to the electronic limitations of the detection system. The analysis of the total events curves shows the typical behavior of scintillator-based detection systems [7]. An approximately linear regime (0–80 MBq, in this study) is observed, in which dead-time, pulse pile-up, and electronic limitations are negligible, and both the scintillator and the electronics respond proportionally to the event rate.

Above 80 MBq, the limitations associated with dead-time, pile-up, and electronics begin to reduce the overall detection efficiency, leading to a sublinear behavior, followed by a peak and a subsequent decrease in the count rate. The true events curves present behavior similar to that of the total events curves.

The random events curves exhibit a distinct behavior compared to total and true events. Initially, a supralinear (apparently quadratic) behavior is observed up to 50 MBq, which is consistent with the work of Oliver and Rafecas (2016) [8]. However, as the activity continues to increase, dead-time effects and electronic limitations begin to reduce the effective rate of recorded events, leading to a slowdown in growth and a tendency toward saturation.

Unlike true and total events, random events do not show a pronounced decrease after a well-defined peak; instead, they tend to stabilize or increase more slowly. With the reduction in the overall detection efficiency of the system and the quadratic nature of random

OPEN ACCESS

coincidence generation, random events tend to predominate at high activity levels. The NEC curves also show behavior similar to total and true events. However, since NEC essentially represents a signal-to-noise ratio, the faster increase in random events causes a slight shift of the NEC peak toward lower activity values compared to the peaks of the true events curves.

4. CONCLUSIONS

The results obtained demonstrate that phantom volume significantly influences the (kCPS) to activity (MBq) conversion coefficient. A reduction in detection efficiency was observed in the larger phantoms, indicating an inverse relationship between phantom size and count efficiency in the temporal mode. This variation underscores the importance of considering phantom geometry in calibration and quantitative procedures in preclinical PET imaging studies to ensure greater accuracy in the analysis.

This work resulted in 3 new phantoms of different volumes that were incorporated into routine laboratory work. These phantoms will allow for greater reliability in quantitative analyses of experiments in general, considering their respective proportions.

ACKNOWLEDGMENT

The authors gratefully acknowledge CDTN/CNEN for providing access to research laboratories and supporting this work. We also thank Dr. Eduardo Sarmento Valente for his assistance in the fabrication of the phantoms, Dr. Bruno Melo Mendes for sharing information and clarifying technical questions, and coauthors Drs. Rodrigo Modesto Gadelha Gontijo and Andrea Vidal Ferreira for their guidance and support during the laboratory experiments. We further thank our colleague Anna Clara Moreira da Silva for her assistance in the laboratory during the experiments.

OPEN ACCESS

FUNDING

This work was supported by CNPq through a Scientific Initiation scholarship, which enabled the experiments to be carried out.

CONTRIBUTORSHIP

Conceptualization: A.V.S., A.V.F.

Investigation: A.V.S., R.M.G.G.

Writing – original draft: A.V.S

Writing – review and editing: A.V.S., A.V.F., R.M.G.G., M.B.M.

Methodology: A.V.S., A.V.F., R.M.G.G.

Formal analysis: A.V.S., A.V.F., M.B.M.

Resources: A.V.F., R.M.G.G., M.B.M.

Supervision: A.V.F.

CONFLICT OF INTEREST

All authors declare that they have no conflicts of interest.

DATA AVAILABILITY STATEMENT

The datasets generated and analyzed during the current study are available from the corresponding author upon reasonable request.

OPEN ACCESS

CC BY

REFERENCES

[1] SAHA, G. B. **Basics of PET Imaging: Physics, Chemistry, and Regulations**. 2nd ed. Cham: Springer, 2010.

[2] GONTIJO, R. M. G. Proposta de Programa de Garantia da Qualidade para Imagem Molecular Pré-Clínica. 2019. **Tese** (Doutorado em Ciência e Tecnologia das Radiações, Minerais e Materiais) – Centro de Desenvolvimento da Tecnologia Nuclear, Comissão Nacional de Energia Nuclear, Belo Horizonte.

[3] MACDONALD, L. R.; HARRISON, R. L.; ALESSIO, A. M.; HUNTER, W. C. J.; LEWELLEN, T. K.; KINAHAN, P. E. Effective count-rates for PET scanners with reduced and extended axial field of view. **Physics in Medicine & Biology**, Bristol, v. 56, n. 12, p. 3629-3643, 2011.

[4] NEMA, National Electrical Manufacturers Association. Performance Measurements of Small Animal Positron Emission Tomographs**. NEMA Standard Publication NU 4-2008**, 2008.

[5] BERGERON, M.; *et al.* Imaging performance of LabPET APD-based digital PET scanners for pre-clinical research. **Physics in Medicine and Biology**, v. 59, n. 3, p. 661–678, 2014. DOI: 10.1088/0031-9155/59/3/661.

[6] GONTIJO, R. M. G.; FERREIRA, A. V.; SILVA, J. B.; MAMEDE, M. Performance based on NEMA NU-4 2008 standard of CDTN/CNEN's small animal PET scanner. **Brazilian Journal of Radiation Sciences**, Belo Horizonte, v. 10, n. 3, p. 1-17, 2022.

[7] KNOLL, G. F. **Radiation detection and measurement.** Hoboken: John Wiley & Sons, 2010.

[8] OLIVER, J. F.; RAFECAS, M. Modelling random coincidences in positron emission tomography by using singles and prompts: a comparison study. **PLOS ONE**, San Francisco, v. 11, n. 9, e0162096, 2016.

LICENSE

This article is licensed under a Creative Commons Attribution 4.0 International License, which permits use, sharing, adaptation, distribution and reproduction in any medium or format, as long as you give appropriate credit to the original author(s) and the source, provide a link to the Creative Commons license, and indicate if changes were made. The images or other third-party material in this article are included in the article's Creative Commons license, unless indicated otherwise in a credit line to the material.
To view a copy of this license, visit http://creativecommons.org/ licenses/by/4.0/.